metals

MDPI

Article

Functionalisation of the Aluminium Surface by $CuCl_2$ Chemical Etching and Perfluoro Silane Grafting: Enhanced Corrosion Protection and Improved Anti-Icing Behaviour

Peter Rodič [1], Matic Može [2], Iztok Golobič [2] and Ingrid Milošev [1,3,*]

[1] Department of Physical and Organic Chemistry, Jožef Stefan Institute, Jamova c. 39, 1000 Ljubljana, Slovenia; peter.rodic@ijs.si
[2] Faculty of Mechanical Engineering, University of Ljubljana, Aškerčeva c. 6, 1000 Ljubljana, Slovenia; matic.moze@fs.uni-lj.si (M.M.); iztok.golobic@fs.uni-lj.si (I.G.)
[3] Valdoltra Orthopaedic Hospital, Jadranska c. 31, 6280 Ankaran, Slovenia
* Correspondence: ingrid.milosev@ijs.si

Abstract: This study aimed to prepare a facile hierarchical aluminium surface using a two-step process consisting of chemical etching in selected concentrations of $CuCl_2$ solution and surface grafting through immersion in an ethanol solution containing 1H, 1H, 2H, 2H-perfluorodecyltriethoxysilane. The goal was to achieve superhydrophobic characteristics on the aluminium surface, including enhanced corrosion resistance, efficient self-cleaning ability, and improved anti-icing performance. The surface characterisation of the untreated aluminium and treated in $CuCl_2$ solutions of different concentrations was performed using contact profilometry, optical tensiometry, and scanning electron microscopy coupled with energy dispersive spectroscopy to determine the surface topography, wettability, morphology, and surface composition. The corrosion properties were evaluated using potentiodynamic measurements in simulated acid rain solution and salt-spray test according to ASTM B117-22. In addition, self-cleaning and anti-icing tests were performed on superhydrophobic surfaces prepared under optimal conditions. The results showed that the nano-/micro-structured etched aluminium surface with an optimal 0.5 M concentration of $CuCl_2$ grafted with a perfluoroalkyl silane film achieved superhydrophobic characteristics, with water droplets exhibiting efficient corrosion protection, self-cleaning ability, and improved anti-icing performance with decreased ice nucleation temperature and up to 545% increased freezing delay.

Keywords: superhydrophobic surface; corrosion protection; self-cleaning; anti-icing

Citation: Rodič, P.; Može, M.; Golobič, I.; Milošev, I. Functionalisation of the Aluminium Surface by $CuCl_2$ Chemical Etching and Perfluoro Silane Grafting: Enhanced Corrosion Protection and Improved Anti-Icing Behaviour. *Metals* **2024**, *14*, 1118. https://doi.org/10.3390/met14101118

Academic Editor: Changdong Gu

Received: 9 September 2024
Revised: 24 September 2024
Accepted: 25 September 2024
Published: 1 October 2024

1. Introduction

Aluminium is a lightweight metal widely used in various industries due to its favourable properties. Due to its low density, it is an excellent choice for applications where weight is critical, such as in the aerospace and automotive industries [1–3]. Although the aluminium surface is coated by a natural oxide layer (Al_2O_3) that is formed spontaneously when aluminium is exposed to oxygen, several surface treatments based on the application's requirements are essential to enhance mechanical properties and corrosion resistance [4,5]. Corrosion protection for aluminium involves using various systems and techniques to prevent or minimise metal degradation due to environmental factors. The most commonly studied corrosion protection systems for aluminium are anodising [6,7], conversion coatings [4,8–10], and organic-inorganic sol-gel coatings [11–13]. Furthermore, resistance to ice accumulation on aluminium surfaces is of interest for many engineering systems and vehicles, ranging from protecting heat pump evaporators from frost to preventing icing on aircraft [14–16].

One possible way to functionalise the aluminium surface is to make it superhydrophobic. Despite numerous studies in the past decade focusing on surface treatments for

achieving superhydrophobic surfaces with outstanding performance [17–21], there remains a challenge to produce a convenient, environmentally friendly, and uncomplicated method for grafting [20,22]. In recent years, innovative materials with exceptional surface properties have been extensively researched in surface treatment [21]. The development of superhydrophobic surfaces has gathered significant attention due to their promising applications in various fields [18,20,21,23,24]. Superhydrophobicity refers to the extreme water-repellent property of a surface, causing water droplets to bead up and roll off easily (the water contact angle of the droplet on the surface has to be larger than 150°, and the sliding angle smaller than 10°) [21,25]. Superhydrophobic aluminium surfaces have proven particularly interesting for their lightweight, cost-effective, and corrosion-resistant properties [23,24,26]. Superhydrophobic surfaces have high potential for applications in different fields because of their excellent properties, ranging from corrosion protection and self-cleaning materials [23,27,28] to anti-icing coatings [25–27,29–31]. The enhanced corrosion protection is also related to reduced wettability with trapped air in the modified surface topography, which prevents the aggressive ions from reaching the aluminium surface, consequently offering an efficient mechanism for corrosion protection [17,18,24,27,29,32].

The naturally passivated aluminium surface is hydrophilic; therefore, surface treatment is needed to reduce its wettability [26,31]. Various methods can be employed to create superhydrophobic surfaces, including the sol-gel process [33], anodic oxidation [34], chemical vapour deposition [35], and chemical etching [26,36]. However, when considering the practical application of such coatings, there is a need for operationally simple, cost-effective methods with a short operation time. The wettability of a solid surface depends on two primary factors: surface roughness and surface chemistry. From this perspective, one of the most straightforward, economical, and environmentally acceptable approaches involves chemical etching (texturing) to generate a roughened surface, followed by grafting a low-surface-energy organic material such as fatty acid [32,37] or alkyl and perfluoroalkyl silanes [26,27,31].

The chemical etching of aluminium and its effect on corrosion properties have been extensively studied, with various methodologies employing a range of reagents to achieve desired surface characteristics. Typically, this process involves the use of strong acid solutions such as hydrochloric acid (HCl) [36,37], and sulphuric acid (H_2SO_4) [38]. Also, mixtures like hydrochloric acid, hydrogen peroxide (HCl/H_2O_2) [26], and Beck's solution (HCl/HF) [39] are commonly used due to their effectiveness in producing fine surface features. On the other hand, alkaline solutions, such as sodium hydroxide (NaOH) [27,32], are also frequently utilised in the etching process. Surface etching can also be performed using solutions of metal chlorides, which serve as effective etchants. Common examples include sodium chloride (NaCl), iron chloride ($FeCl_3$) [31], and copper chloride ($CuCl_2$) [40]. Each etching solution enables precise control over the resulting surface topography and creates hierarchical structures.

This study focused on a two-step process involving surface texturing using copper chloride ($CuCl_2$), which has been studied less despite a comparative analysis of different etchants revealing that $CuCl_2$ yields the best performance [36]. $CuCl_2$ has been chosen for its effectiveness in creating nanostructures on aluminium surfaces [40]. Song et al. [35,40] demonstrated the successful use of Cu ions for aluminium surfaces via a chemical deposition process, revealing enhanced hydrophobic properties. Despite its potential, the etching procedure using $CuCl_2$ has received comparatively less attention than other acid or alkaline chemical etching processes [26,31,32,36,39], presenting an opportunity for further development.

Chemically etched hydrophobic surfaces for anti-icing applications have also been proposed, using a range of etching agents and processing conditions. Fenero et al. [41] developed omniphobic surfaces on 1050 aluminium alloy samples by combining chemical etching in a 14 wt.% aqueous ferric chloride solution at 50 °C for various periods of time, followed by surface modification with perfluoro(polypropyleneoxy)-methoxypropyltrimethoxysilane. The surfaces exhibited superhydrophobicity and strong oleophobic properties and were demonstrated to increase the freezing delay 20-fold compared to untreated surfaces.

Han et al. [42] treated aluminium substrates in hot water for various durations to induce nanostructure growth, followed by the grafting of octadecyltrichlorosilane to achieve superhydrophobic properties. The longest etching time of 2 h was found to grant the best anti-icing properties. Liao et al. [38] used a two-step etching process to modify 1060 aluminium alloy samples by first immersing the sample in 1 M $CuCl_2$ for 8 s, followed by rinsing and etching for 10 s in concentrated HCl. After grafting with hexadecyltrimethoxy, the samples exhibited superhydrophobicity and significantly limited the growth of glaze ice during a custom-designed 50-min test. Peng et al. [43] treated SAE AMS 4037 aluminium alloy plates by etching them in a solution of HCl and H_2O_2 with different molar ratios of both agents. The modification was completed by immersion into hot water and later by grafting the surfaces with stearic acid to achieve superhydrophobicity, self-cleaning behaviour, and reduced ice accumulation. Ruan et al. [44] used several etching solutions to functionalise 5052 aluminium alloy, including diluted Beck's dislocation etchant and a mixture of $FeCl_3$ and HCl. One-step chemical etching with a 1:1 volume mixture of 40 wt.% $FeCl_3$, 6 wt.% HCl aqueous solution, and 10 wt.% lauric acid ethanol solution at 40 °C was identified as the optimal processing pathway to achieve desirable superhydrophobic and anti-icing properties. Zuo et al. [38] etched 1060 aluminium alloy in 1 M $CuCl_2$ aqueous solution, followed by immersion in hot water and hydrophobisation with hexadecyltrimethoxy silane. The produced coral-like superhydrophobic structure displayed excellent anti-icing properties. Wang et al. [45] used a mixture of HF and HCl in an aqueous solution and dip coating with 1H,1H,2H,2H-perfluorodecyltriethoxysilane to produce a superhydrophobic surface on 1060 aluminium alloy samples. The functionalised surfaces exhibited resistance to impacting subcooled water droplets, significantly reduced ice adhesion, and favourable resistance to degradation after cyclical icing/de-icing.

This paper comprehensively investigates a facile two-step process to produce superhydrophobicity on aluminium surfaces. First, a hierarchical micro/nanostructure was formed on the aluminium surface through an etching procedure in a $CuCl_2$ solution. Subsequently, grafting was performed using a solution of 1H,1H,2H,2H-perfluorodecyltriethoxysilane (FAS-10) in ethanol as a low-surface energy material. Silane grafting introduces a hydrophobic chemical coating (due to a low surface energy of groups such as CH, CF_2, and CF_3 in the chain), further reducing the surface energy and enhancing water repellency [46]. Superhydrophobic properties serve as the foundation for diverse surface functionalities. In this context, the dynamic characterisation of water droplets on the surface becomes crucial for understanding self-cleaning and anti-icing properties. The research delved into surface morphology and composition to investigate the relationships between etching solution concentration and grafting. Exposure to a corrosive environment is crucial for selecting the most suitable aluminium surface and appropriate protective measures. A key novelty of this research lies in examining the dynamic behaviour of water droplets on the superhydrophobic film. This aspect provides valuable insights into functional properties, such as the self-cleaning ability for solid pollutants, icing delay, ice nucleation temperature reduction, and the delay in ice melting.

2. Materials and Methods

2.1. Metal Substrates, Chemicals and Surface Preparation

A 1 mm thick aluminium sheet with a purity of 99.0% was distributed from Goodfellow Cambridge Ltd, Huntingdon, UK (abbreviated as REF). The sheet was cut into plates of 40 mm × 40 mm. The surface was ground using a Struers LaboSystem LaboPol-20 machine subjected to 1000, 2000, and 4200 grit SiC abrasive papers (supplied by Struers ApS, Ballerup, Denmark) in the presence of tap water.

Fabricating a superhydrophobic aluminium surface involved a two-step process (Figure 1). In the first step, the aluminium was etched for 30 s in a $CuCl_2$ solution at selected concentrations of 0.1, 0.25, 0.5, 0.75, and 1 M. The etching solution consists of copper(II) chloride ($CuCl_2 \times 6H_2O$; powder purity > ACS reagent, 98%, CAS no. 7447-39-4, supplied by Sigma-Aldrich, Steinheim, Germany) and Milli-Q Direct water with a resistivity

of 18.2 MΩ cm at 25 °C (Millipore, Billerica, MA, USA). The solutions were prepared in a volumetric flask to attain a selected concentration.

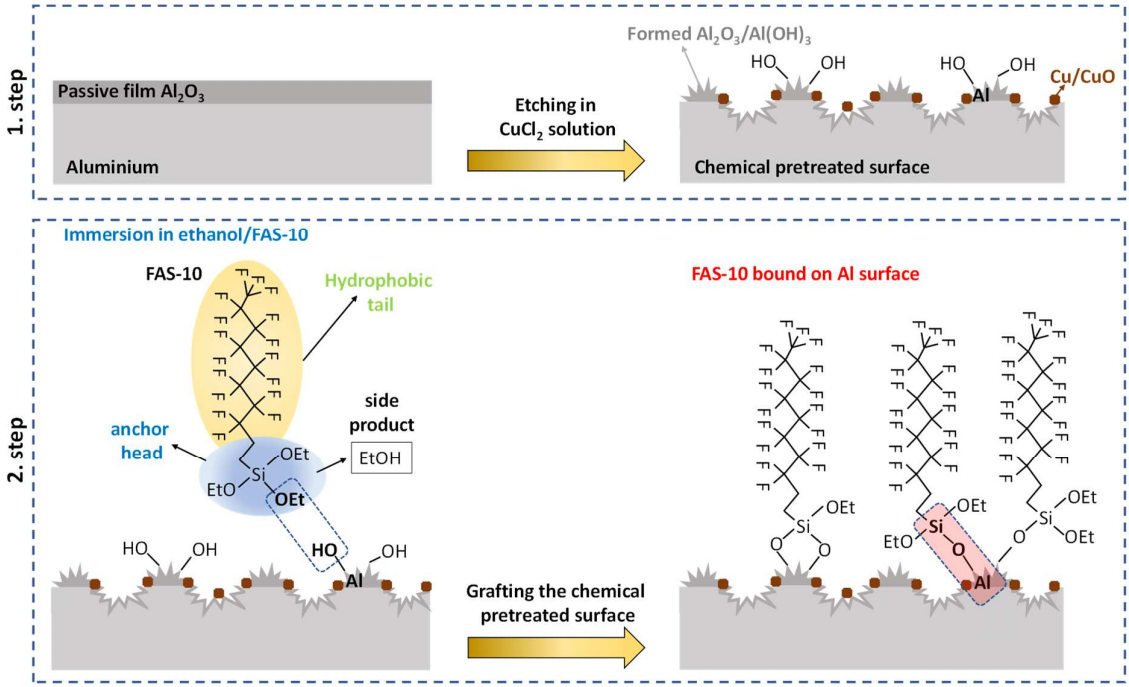

Figure 1. The schematic presentation of a two-step process to form a (super)hydrophobic aluminium surface. Firstly, the aluminium surface undergoes a chemical etching process in a $CuCl_2$ solution (**1. step**), followed by the second step of grafting the surface with perfluoroalkyl silane, FAS-10 (**2. step**).

In the second step, grafting was performed through immersion in a 1 wt.% 1H,1H,2H,2H-perfluorodecyltriethoxysilane, abbreviated as FAS-10 ($C_{16}H_{19}F_{17}O_3Si$, purity > 97%, CAS no. 101947-16-4, distributed by Sigma-Aldrich) ethanol solution (anhydrous ethanol C_2H_5OH, purity > 99.9%, CAS no. 64-17-5, supplied by Sigma-Aldrich), Figure 1.

The aluminium samples were placed at the bottom of the beaker, with the ground surface facing upward. The etching and grafting procedures were carried out at ambient temperature. Following each preparation stage (grinding, etching, grafting), the specimens were thoroughly rinsed with distilled water and immersed in pure ethanol within an ultrasonic bath to eliminate remnants from the grinding or etching processes and other organic compounds on the surface and remove unreacted FAS-10. After each step, the specimens were dried using a compressed nitrogen stream.

2.2. Surface Characterisation

2.2.1. Weight Loss Test

The weight loss test was conducted to assess the effectiveness of the etching process. Weight loss was quantified as the percentage difference in the weight of a clean and dried aluminium sample before and after etching. The measurements were carried out using a digital precision laboratory analytical weighing scale (Mettler Toledo, Columbus, OH, USA, AE200 Analytical Balance) with a precision of 0.1 mg. The evaluation was executed on five parallel samples, and the data are presented as average values along with standard deviations. Linear regression was applied to the obtained data to determine the etching rate, as indicated by the slope of the curve.

2.2.2. Surface Topography

Following varying etching durations, the 3D surface topography of etched aluminium surfaces was assessed at three randomly selected locations. This analysis utilised a stylus contact profilometer, specifically the Bruker DektakXT model (Bruker, Billerica, MA, USA), equipped with a 2 µm tip, operating in a soft-touch mode with a force of 1 mN. The measured surface area was 1 mm × 1 mm, with a vertical analysis range of ± 65.5 µm and a vertical resolution of 0.167 µm/point. The collected data were analysed using TalyMap Gold 6.2 software. The results are presented as 3D plots, with corresponding mean surface roughness (S_a) calculated according to the standard ISO 25178-1:2016 [47] reported as average values and standard deviations.

2.2.3. Wettability

Water contact angles were measured at room temperature using the static sessile-drop method on a Krüss FM40 EasyDrop (KRÜSS GmbH—Germany, Borsteler Chaussee 85, 22453 Hamburg, Germany) contact-angle measuring system. A small liquid droplet (4 µL) generated at the syringe tip was carefully deposited onto the treated aluminium surface. Digital images of the droplet silhouette were captured using a high-resolution camera, and the contact angle was determined by numerically fitting the droplet image through associated protocol software for drop shape analysis. The reported values represent the average of at least five measurements taken from various randomly selected areas and are presented as average values with corresponding standard deviations.

2.2.4. SEM/EDS Characterisation

The morphology and composition of aluminium etched in $CuCl_2$ and grafted with FAS-10 were analysed by focused ion beam/scanning electron microscopy (FEI Helios NanoLab 600 Dual-beam, ThermoFisher Scientific, Waltham, MA, USA). Before analysis, the samples were coated with a few nanometers of a thin carbon layer. SEM imaging was conducted by a secondary electron mode (SEI mode) using an ion conversion and electron (ICE) detector at acceleration voltage of 10 kV. EDS analyses were performed at 10 kV in an area analysis mode. The data are presented as atomic percentages (at.%).

2.2.5. Corrosion Testing

The corrosive medium was prepared in a volumetric flask containing 0.2 g Na_2SO_4 + 0.2 g $NaHCO_3$ + 0.2 g $NaNO_3$ in 1 L of water. The pH value of the solution was adjusted to 5.0 using 0.1 M H_2SO_4 solution. This solution simulates acid rain conditions [48].

Electrochemical measurements were performed at ambient temperature (~23 °C) in a three-electrode corrosion cell (volume 250 mL). The working electrode was a bare and grafted aluminium substrate with a 1.0 cm^2 surface exposed to the corrosive medium. A carbon rod was employed as the counter electrode, while the reference electrode used was a saturated Ag/AgCl electrode (with E = 0.197 V vs. the standard hydrogen electrode).

Electrochemical tests were conducted using an Autolab PGSTAT 204M potentiostat/galvanostat from Metrohm Autolab in Utrecht, The Netherlands, controlled by Nova 2.1 software. The samples were allowed to stabilise under open circuit conditions for 1 h, and the stable quasi-steady state potential reached at the end of this period was identified as the open circuit potential (E_{oc}). Following stabilisation, electrochemical measurements were performed. Potentiodynamic measurements involved a potential scan rate of 1 mV/s, starting from −250 mV to E_{oc}, with the potential subsequently increased in the anodic direction. Measurements were conducted at least in triplicate for each sample, and the representative measurement was selected. Tafel approximation was applied to polarisation curves to obtain corrosion parameters, including corrosion current density (i_{corr}) and corrosion potential (E_{corr}). The breakdown potential (E_{bd}) was determined as the potential in the passive region where the current density gradually increased.

Accelerated corrosion testing in a salt-spray chamber was performed for the selected samples: ground, etched, and treated (etched + grafted) aluminium. The test was performed

in a 0.750 m^3 salt-spray chamber (HKT 750 BASIC-LINE, KÖHLER (Köhler Automobiltechnik GmbH, Lippstadt, Germany) operating according to the ASTM B117-22 standard [49]. pH of NaCl solution (50 ± 1% g/L) was set to between 6.0 and 6.5 at room temperature to give values of pH between 6.5 and 7.2 after heating the solution to 35 °C ± 2 °C, which was the temperature of the chamber. The temperature in the chamber was set at 35 °C ± 2 °C. The samples were positioned in a holder, ensuring a surface tilt at an angle of 30°. At selected time intervals, the samples were removed, rinsed with distilled water, and then dried using a stream of nitrogen. The test lasted 7 days. The changes in the sample appearance were monitored as a function of exposure time and photographed with a digital camera at selected times: 1 h, 24 h, and 168 h (7 days).

2.2.6. Self-Cleaning Ability

Self-cleaning tests were conducted on untreated and treated aluminium samples measuring 40 mm × 40 mm. The procedure involved placing the aluminium sample on a horizontal stage tilted at 2°. To simulate solid pollution, the aluminium surface was covered with graphite multiwalled nanotubes (Carbon > 95%, length 1–10 µm, PlasmaChem GmbH, Berlin, Germany). Subsequently, a water droplet was released onto the surface from a height of 2 cm. The movement of solid pollution with the water droplet was recorded using a digital camera to assess pollutant removal after the water droplet rolled off the surface.

2.2.7. Anti-Icing Ability

The investigation into the anti-icing characteristics encompassed untreated (REF) and treated aluminium samples, each measuring 40 mm × 40 mm, subjected to subcooled conditions. Three types of tests were conducted. Firstly, the freezing delay was recorded at multiple surface temperatures. This was followed by evaluation of the ice nucleation temperature. Finally, the ice-melting kinetics were evaluated.

For freezing delay and ice nucleation temperature measurements, the same custom-designed experimental method was utilised. The experimental setup was based around a transparent enclosed experimental chamber, which provided a controlled atmosphere. The chamber was positioned on a tilting table, allowing for the horizontal alignment of the sample to prevent a droplet roll-off. The humidity inside was controlled using silica gel desiccant to reduce the relative humidity below 15%. The sample was positioned in the center of the chamber on a 2-stage thermoelectric element. Thermal paste was used at the contact point between the thermoelectric element and the sample to improve the heat transfer. The thermoelectric element was operated via a PID controller (Meerstetter TEC-1123-HV, Meerstetter Engineering GmbH, Rubigen, Switzerland) and a type K thermocouple was used to monitor the temperature of the sample surface. Heat was dissipated from the hot side of the element through a water block connected to a closed water-cooling loop. Throughout the measurements, the temperature and the humidity inside the chamber were monitored to ensure comparable experimental conditions for both tested samples.

To measure the freezing delay time, we applied 15 water droplets (V = 7 µL) onto the surface of the sample at room temperature with an automatic pipette. The measurements were conducted by cooling the sample with the thermoelectric element at a rate of 1 K/s, with target temperatures of −15 °C, −17.5 °C, and −20 °C. Once all droplets on the surface had frozen, the recording was stopped, and the samples were heated back to room temperature. Three repetitions were conducted for each target temperature. A camera from the bird-eye perspective was used to record the freezing process, and the footage was analysed to determine how long it took each droplet on the surface to freeze at the given target temperature. It should be noted that the reported freezing delay time also includes the time it took the sample to reach the target temperature (approx. 45 s). Furthermore, it should be noted that some droplets froze even before the target temperature was reached.

To measure the nucleation temperature, we also applied 15 water droplets (V = 7 µL) onto the surface at room temperature. Then, the experimental chamber was closed, and cooling of the sample was initiated. These measurements were performed by cooling the

sample with the thermoelectric element at a rate of 0.1 K/s, with a target temperature of −30 °C. Once all droplets on the tested surface froze, cooling was discontinued, and the sample was returned to room temperature. Measurements were repeated three times. A camera from the bird-eye perspective was used to record the freezing process and the recordings were used to correlate the moment of nucleation with the corresponding surface temperature at that moment. Nucleation was clearly observed as a rapid colour change of the water droplet from the initially transparent state to an opaque (white) state.

The ice melting process was additionally followed on ~30 µL droplets, which were delicately deposited onto the horizontal substrates. Following a one-hour exposure to a freezer (−15 °C), the samples were given to ambient room temperature. The melting (de-icing) kinetics were assessed by analysing droplet temperature on untreated (REF) and treated surfaces, utilising a thermal Fluke Ti55FT Infrared Camera (Everett, WA, USA).

3. Results and Discussion

3.1. Surface Characterisation after Treatment

3.1.1. Weight Loss Test

Aluminium etching as a function of $CuCl_2$ concentration at constant etching time (30 s) was quantitively evaluated using weight loss measurements (Figure 2). The sample weight is reduced proportionally with the concentration of $CuCl_2$, due to two factors: (a) solution pH and the presence of Cl^- ions and (b) presence of Cu ions forming chemical (redox) reactions.

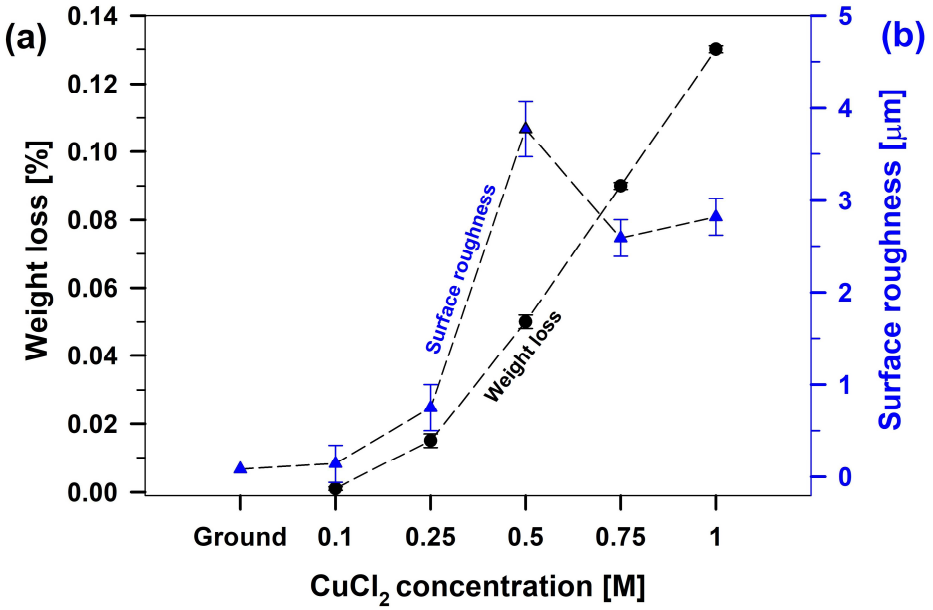

Figure 2. (**a**) The mass loss of aluminium after the etching process as a function of concentration of $CuCl_2$ solution. Etching time was 30 s. (**b**) The surface roughness determined from 3D surface plots obtained with a contact profilometer (Figure 3) as a function of $CuCl_2$ concentration.

When dissolved in water, $CuCl_2$ dissociates into Cu^{2+} and $2Cl^-$ ions. A reversible hydrolysis equilibrium reaction occurs between Cu^{2+} ions and water molecules, yielding H^+ ions and acidifying the solution, as reaction (1) denotes.

$$Cu^{2+} + 2H_2O \rightarrow Cu(OH)^+ + H_3O^+ \quad (1)$$

$$2Al^{3+} + 6Cl^- \rightarrow 2AlCl_3 \quad (2)$$

The H_3O^+ produced by this reaction makes the solution acidic with pH below 2.5. The passive film on the aluminium surface is not stable at pH below ~4 [50]. The soluble Cl^-

ions react with aluminium and form aluminium chloride ($AlCl_3$), reaction (2). Low pH and the present Cl^- ions in $CuCl_2$ solution present a strong etching solution.

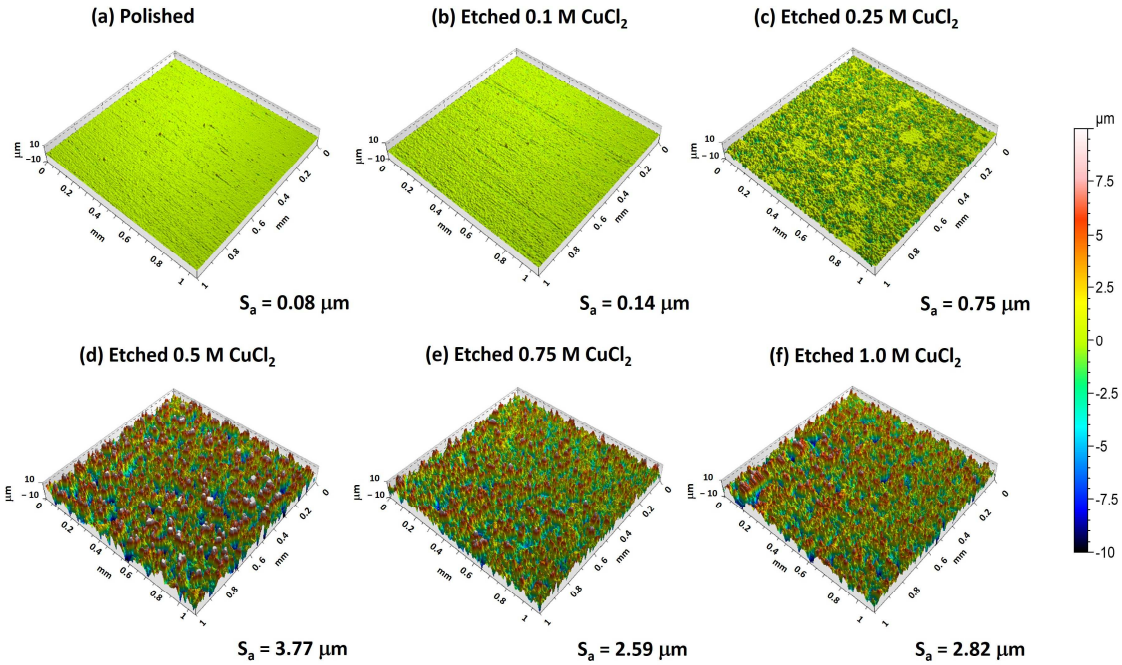

Figure 3. 3D surface topography images of aluminium surface etched as a function of $CuCl_2$ concentration. The surface roughness determined from 3D surface plots is given as S_a and presented in a graph in Figure 2.

The mechanism of the chemical etching is also based on chemical (redox) reactions between the passivated aluminium surface and copper ions in aqueous solution, establishing an aluminium-copper (Al-Cu) cell (3).

$$2Al + 3Cu^{2+} \rightarrow 2Al^{3+} + 3Cu \quad (3)$$

During etching, the aluminium is oxidised and dissolved into solution; at the same time, Cu^{2+} is reduced to Cu and deposited into the etchant solution [36,51,52].

The etching process starts on the aluminium surface during immersion in $CuCl_2$ solution. The area and depth of the etched surface depend on the concentration of $CuCl_2$. The experiments confirmed that the etching is less aggressive at low concentrations (up to 0.25 M) due to the relatively resistant passive layer of Al_2O_3. At higher concentrations (above 0.25 M), the mass loss becomes more pronounced, Figure 2. The kinetics of the reaction are related to the diffusion process between substrate and etchant solution. A linear increase in weight loss at $CuCl_2$ concentrations above 0.25 M confirms the reduced passive behaviour of aluminium due to a high aggressiveness of $CuCl_2$ solution.

The chemical etching process of aluminium with $CuCl_2$ as a function of etching concentration can be described in more detail. At the initial stage, corrosive chloride ions (Cl^-) with a small ionic radius initiate the degradation of the passive aluminium oxide layer (Al_2O_3). This process is retarded at low concentrations, but at higher concentrations (above 0.25 M), they are susceptible more to destruction. Subsequently, Cl^- ions come into contact with aluminium (Al) substrates by permeating through the deteriorated oxide layer, instigating a reaction with the elemental aluminium to form aluminium chloride ($AlCl_3$). Therefore, the linear behaviour of the etching is observed from 0.25 up to 1 M.

During this process, greater concentrations of Cu^{2+} ions undergo reduction to their elemental form and are subsequently precipitated onto the aluminium surfaces or form insoluble salts.

The more pronounced etching process at greater $CuCl_2$ concentrations can be seen visually due to the aggressive displacement reaction between the freshly ground aluminium surface and etching solution (seen as bubble formation related to hydrogen evolution and heating of the etchant solution, reaction (4)).

$$2Al + 6H_2O \rightarrow 2Al(OH)_3 + 3H_2 \quad (4)$$

Regions where H_2 bubbles are formed retard the deposition of copper due to the absence of available Cu^{2+} ions, impeding the growth of copper towards the surface. As a result, copper deposition occurs non-uniformly in the form of a thin film.

After removing the aluminium sample from the etching solution and exposing it to the environment, the aluminium surface reacts spontaneously with oxygen/humidity during rinsing with water, which causes the formation of a fresh aluminium/copper oxide/hydroxide film containing OH^- groups (Figure 1).

3.1.2. Surface Topography

3D surface topography images of the aluminium surface etched as a function of $CuCl_2$ concentration are presented in Figure 3, together with surface roughness values.

The surface roughness (S_a) as a function of the $CuCl_2$ concentration at constant etching time (30 s) is quantitatively presented in Figure 2b. The ground aluminium has a low surface roughness, $S_a = 0.08 \pm 0.03$ µm. The surface roughness of the 0.1 M $CuCl_2$-etched aluminium sample was almost doubled to $S_a = 0.14 \pm 0.2$ µm and continued to increase linearly up to a concentration of 0.5 M to $S_a = 3.77 \pm 0.3$ µm. Especially at 0.25 M, there are areas where some islands of unetched areas are seen, which reflect the non-uniform etching process at lower concentrations (Figure 3c). At 0.5 M concentrations, the islands were seen only as small spikes. At greater concentrations (0.75 and 1 M), the roughness decreased and reached similar values of $S_a = 2.59$ and 2.82 ± 0.4 µm. The decrease in surface roughness is related to the complete removal of the native passive film (no islands/spikes remain on the etched surface). The increase in surface roughness correlates with weight loss (Figure 2); low changes at lower concentrations, and greater changes at concentrations above 0.5 M $CuCl_2$. Therefore, both parameters can be controlled by the etchant concentration.

The 3D surface plots show that the surface topography of the surfaces is strongly related to the concentration of $CuCl_2$ (Figure 3). Moreover, 3D surface plots show that the number of large pits increased at a concentration of 0.5 M $CuCl_2$.

3.2. Surface Wettability

The transition from a (super)hydrophilic surface of the non-treated Al sample to a (super)hydrophobic surface of the $CuCl_2$-etched and FAS-10-grafted samples was followed utilising water contact angle (WCA) measurements.

The untreated aluminium surface (REF) exhibited hydrophilicity (these data were measured but are not shown in the figure), with a WCA of approximately 69°, attributed to a naturally formed oxide layer from exposure to air or moisture. Grinding and etching in $CuCl_2$ solution enhanced the wettability of aluminium, creating a rough, hydroxylated surface (due to the formation of Al–OH groups). The etched aluminium displayed superhydrophilicity, with a WCA of only a few degrees (not shown in the figure).

Grafting ground aluminium substrates with FAS-10 increased the water contact angle to 123°, highlighting the necessity of surface etching for achieving a superhydrophobic surface (Figure 4). The static WCAs exhibited a substantial rise with increasing $CuCl_2$ etching concentration (Figure 4). This increase can be attributed to two interconnected phenomena: the enhancement of micro/nano roughness due to prolonged etching (Figure 3) and the presence of low surface energy molecules such as FAS-10. Following etching in 0.1 M $CuCl_2$, the water contact angle reached 128°. With etching in 0.5 M $CuCl_2$, all measured contact angles exceeded 150°, demonstrating superhydrophobicity. Further increases in etching concentration did not yield additional improvements in the water contact angle, because surface roughness slightly decreased from 3.77 (0.5 M) to 2.59

(0.75 M $CuCl_2$) and to 2.89 (1 M $CuCl_2$) (Figure 3) as a result of aggressive chemical etching where small pits/holes merged into larger valleys. Therefore, it can be concluded that etching the surface with 0.5 M $CuCl_2$ and grafting for 30 min in FAS-10 solution were optimal conditions to obtain superhydrophobic properties with high water repellence.

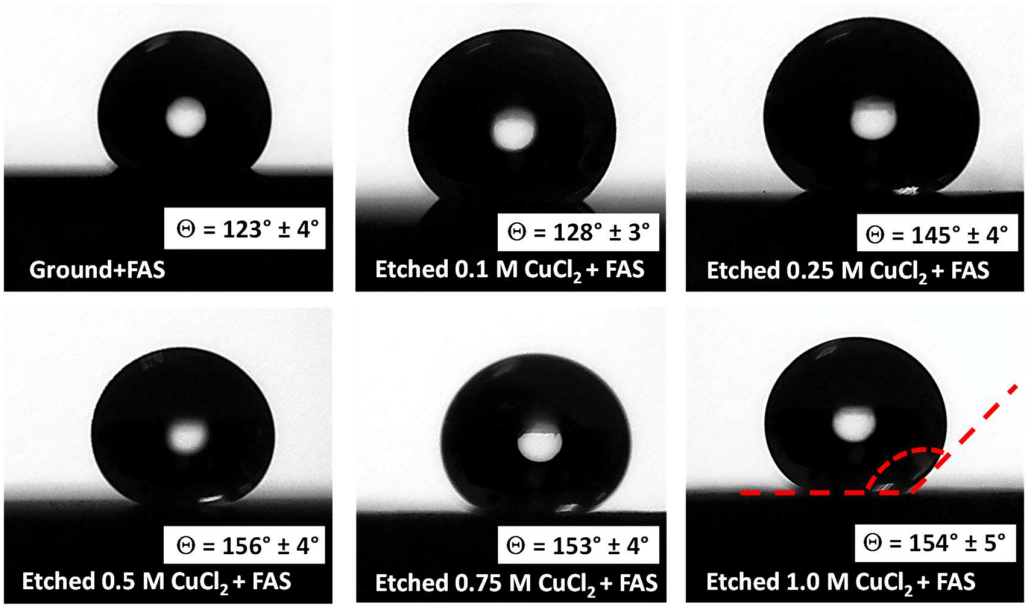

Figure 4. Water contact angles measured for water droplets on an aluminium surface etched for 30 s in selected concentrations of $CuCl_2$ and grafted for 30 min in 1 wt.% ethanol FAS-10 solutions. The results are presented as mean values ± standard deviations.

The chemical modification of the surface explains the observed decrease in wettability of etched and grafted samples. During the second step, denoted as grafting, the reaction between freshly formed hydroxylated aluminium (Al–OH) and $(CH_3CH_2O)_3$–Si–$(CH_2)_2(CF_2)_7CF_3$ (FAS-10) occurred (Figure 1). The reaction between the anchor of FAS-10, –OCH_2CH_3 (OEt-ethoxy group) representing a hydrolysable ethoxy group and –$(CH_2)_2(CF_2)_7CF_3$, and a non-hydrolysable perfluoroalkyl chain results in the formation of the surface film (Figure 1). The interfacial condensation reactions take place between the alkoxy and hydroxy groups of the etched aluminium, leading to covalent binding between the silane head of the FAS-10 molecule and aluminium surface according to reaction (5), with ethanol as the side product:

$$Al–(OH)_3 + (CH_3CH_2O)_3–Si–(CH_2)_2(CF_2)_7CF_3 \rightarrow Al(OH)_2–O–Si–(OCH_2CH_3)_2–(CH_2)_2(CF_2)_7CF_3 + CH_3CH_2OH \quad (5)$$

The Al–OH groups on the freshly $CuCl_2$-etched aluminium surface act as active sites for covalent bonding with the silicon in the FAS-10 molecule, forming –Si–O–Al bonds (Figure 1). The condensation process is an exothermic chemical reaction, facilitating a monodentate interaction between the surface and the fluoro-silane, as reported in the literature [53,54]. This reaction allows the silane head of the FAS-10 molecule to bond with the aluminium surface while the non-polar –$(CH_2)_2(CF_2)_7CF_3$ functional groups are oriented outward, enhancing hydrophobicity (Figure 1).

3.3. SEM/EDS Surface Morphology and Composition

The topography and morphology of ground and etched aluminium in 0.5 M $CuCl_2$ and etched and modified aluminium with FAS-10 were evaluated using scanning electron microscopy (SEM) performing imaging in a secondary electron mode (SEI) using an ICE detector. Etching and grafting were performed under optimal conditions (Figure 4).

SEM analysis revealed numerous tiny pores and defects on the surface of the ground aluminium, likely associated with the mechanical properties of the material and the surface grinding process. Elemental EDS analysis of the surface in the denoted area presented in a pie diagram (Figure 5) indicated that ground aluminium is primarily composed of Al and O, suggesting the presence of a thin aluminium oxide layer on the surface (Figure 5). Carbon was also detected, originating from coating the samples before analysis.

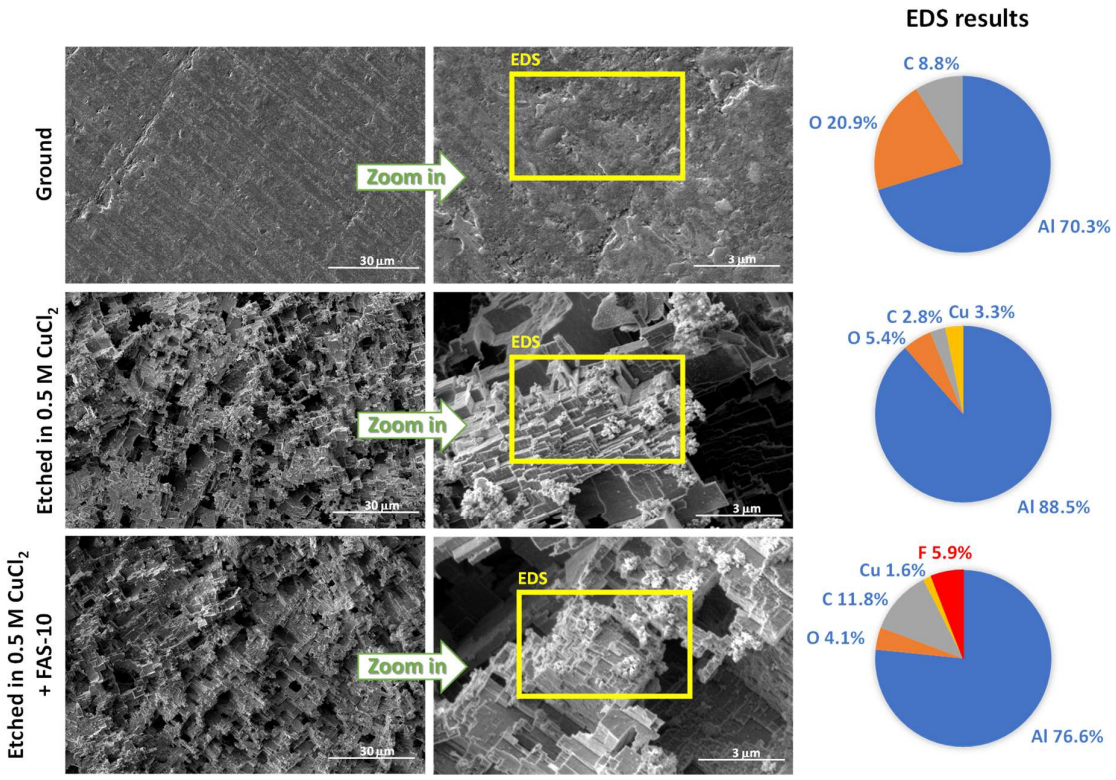

Figure 5. SEM images recorded in SEI mode using an ICE detector of the aluminium surface etched for 30 s in 0.5 M $CuCl_2$ and grafted for 30 min in 1 wt.% ethanol FAS-10 solution. The square positions indicate the areas where the EDS analyses were performed (values in atomic percentage are given in pie charts).

SEM imaging of aluminium after 30 s of etching revealed the formation of micro- and nanostructured surface patterns compared to the ground surface, along with numerous small holes and larger, deep pits (Figure 5). Dispersed rectangular micro-scale pits ranging from 5 to 20 µm in width were observed across the surface. These rectangular pits and the reduction in size of interconnected edges of the nano-hierarchical structure were more apparent at a higher magnification. The evenly distributed rectangular pits contribute to the hierarchical structure. Despite etching, impurities persisted on the surface, as confirmed by SEM ICE images, indicating the presence of residual copper on the aluminium surface. EDS analysis confirmed that Cu is present in a few percentages on the surface (3.3 wt.%), validating the reaction described by reactions (1 and 3), where Cu is partially deposited on the aluminium surface. Notably, chloride ions, which might remain as residues of $AlCl_3$ or $CuCl_2$ etching, were not detected on the treated surface using given experimental EDS parameters, indicating a well-controlled etching process utilised to achieve superhydrophobicity during grafting.

Figure 5 also shows the typical morphology of aluminium etched for 30 s in $CuCl_2$ and subsequently grafted with FAS-10 for 30 min. The organic film formed by grafting is presumed to be nanometer-sized, making it challenging to analyse via contact profilometry or changes in sample weight. Consequently, the etched and FAS-10-grafted surface morphology was investigated using SEM/EDS. The appearance of etched and modified

(etched + FAS-10) aluminium surfaces was very similar, indicating that the FAS-10 layer on the surface is nanometric in thickness, rendering the bound molecules invisible even at higher magnifications. This morphology facilitates the presence of air within the structure, which is crucial for achieving (super)hydrophobic properties.

EDS analysis confirmed the presence of FAS molecules on the modified aluminium surface. The analysis showed that the surface is composed of Al, O, Cu, and F. Al, O, and Cu are connected to Al/Al_2O_3 on the surface, while F is attributed to the FAS molecules bound to the aluminium surface. F originating from FAS-10 was detected in multiple areas on the surface, confirming the efficient grafting during immersion in FAS-10 solution.

The SEM and EDS analyses revealed significant surface changes in aluminium after etching and modification with FAS-10. The etching process introduced micro- and nanostructures along with rectangular pits, while the grafting of FAS-10 resulted in a nanometer-thick organic film. Despite introducing these features, impurities such as copper persisted on the surface. The successful presence of FAS-10 molecules, detected via EDS, confirmed the efficacy of the grafting process, which is essential for achieving the desired superhydrophobic properties.

3.4. Self-Cleaning Ability of the Superhydrophobic Surface

The self-cleaning assessment was conducted on both ground and optimally treated aluminium surfaces (etched + FAS-10) to evaluate the removal of solid pollutants from the surface. Before the test, carbon nanotube particles were deposited on the surfaces to simulate environmental solid pollutants.

Figure 6 illustrates that despite the application of water on the ground aluminium surface, the pollutants remained adhered to it. The surface is wetted, with particles dispersed within the water film. Therefore, the untreated ground aluminium surface exhibits no self-cleaning ability.

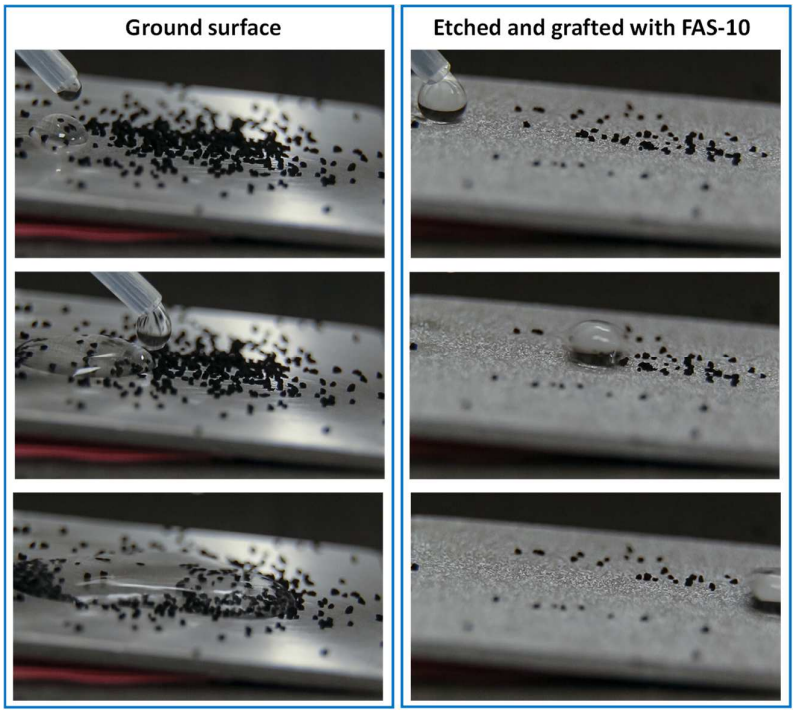

Figure 6. The surface appearance of ground and treated aluminium surfaces (etched for 30 s in 0.5 M $CuCl_2$ and grafted for 30 min in 1 wt.% ethanol FAS-10 solution) covered with carbon particles prior to and after tap water dropping on the surface.

In contrast, no carbon particles or water droplets remained on the treated aluminium surface after water application, as the rolling water droplets effectively removed the par-

ticles (Figure 6). This result demonstrates the superhydrophobic aluminium surface's excellent water-repelling and self-cleaning ability. The water droplets do not penetrate the grooves but are suspended on the micro- and nano-scale pits. As a result, water droplets cannot adhere to the surface and depart quickly without significant distortion. The low adhesion characteristic of the superhydrophobic surface allows droplets to roll off effortlessly, removing various external contaminants, similar to the natural lotus leaf [24,29]. The superhydrophobicity of the etched and FAS-10-grafted surface results from a hierarchically rough surface covered by a film with low surface energy (perfluoro tail). This configuration traps air in "pockets" between the water droplets and the solid surface, minimising their contact and enhancing water repellency.

3.5. Corrosion Protective Performance

The corrosion performance was first evaluated through potentiodynamic polarisation curves recorded in simulated acid rain (0.2 g Na_2SO_4 + 0.2 g $NaHCO_3$ + 0.2 g $NaNO_3$ solution) for ground and treated aluminium samples (Figure 7).

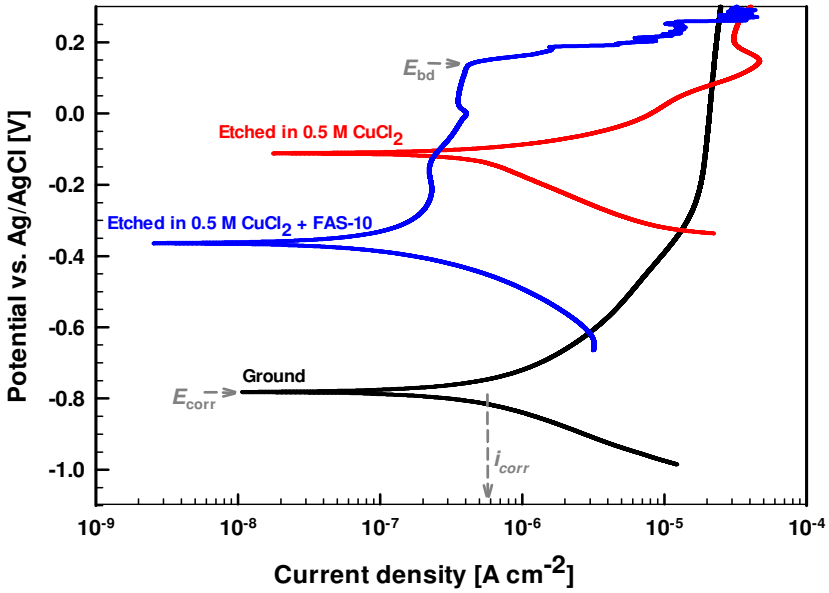

Figure 7. Potentiodynamic polarisation curves for ground and treated aluminium (etched and grafted with FAS-10) measured in simulated acid rain solution (0.2 g Na_2SO_4 + 0.2 g $NaHCO_3$ + 0.2 g $NaNO_3$) after 1 h of immersion.

Ground aluminium exhibited relatively good corrosion resistance in the tested solution, with a corrosion current density (i_{corr}) of 0.62 μA/cm^2 and a corrosion potential (E_{corr}) of −0.78 V. However, in the anodic part of the curve, the current gradually increases to values of 1.8 × 10^{-5} μA/cm^2 and a region with almost constant current was established in the tested media. Based on the results, the corrosion medium containing SO_4^{2-}, HCO_3^-, and NO_3^- ions is slightly less aggressive than a medium with Cl^- ions [55], but such an aluminium surface still needs additional corrosion protection.

Corrosion resistance diminished after etching with $CuCl_2$, indicated by a slight increase in i_{corr} (Figure 7) to 0.72 μA/cm^2. However, E_{corr} was considerably shifted in a more noble direction to −0.12 V, i.e., by almost 660 mV. The decrease in corrosion resistance is most likely attributed to removing the natural passive film after grinding and forming a new surface layer after etching in $CuCl_2$, as presented by reactions (1) and (3). The formed film is less resistant, reducing the effectiveness of surface protection. In addition, changes can also be related to the residuals of Cu that remained on the surface during the etching process, which was determined by SEM/EDS (Figure 5).

In contrast, surface modification after etching led to a substantial decrease in i_{corr} (Figure 7) to 0.11 μA/cm^2 and the E_{corr} was shifted to −0.36 V. The main difference is the established broad passive behaviour with breakdown potential E_{br} at 0.14 V (the potential when current density gradually increases). The difference between E_{corr} and E_{bd} was 500 mV. This indicates a marked improvement in corrosion protection. Similar improvements were also noticed for other two-step chemical etched superhydrophobic coatings [20,26]. The enhancement is attributed to the superhydrophobic surface, which prevents contact between the aluminium surface and corrosive ions in the simulated acid rain solution. Thus, the electrochemical results confirmed that this type of surface modification significantly improves the corrosion properties of aluminium.

The corrosion resistance of ground, etched, and FAS-10-grafted aluminium was also evaluated after different exposure times in a salt-spray chamber (Figure 8). Due to the more demanding corrosion conditions, this test significantly accelerates the corrosion processes on the surface. The passive film on the ground samples provided ineffective protection under harsh conditions. Most of the surface was covered with corrosion products after 24 h of immersion, manifesting as a slightly grey-coloured surface. The amount and surface area of corrosion products increased with exposure time, particularly after 168 h.

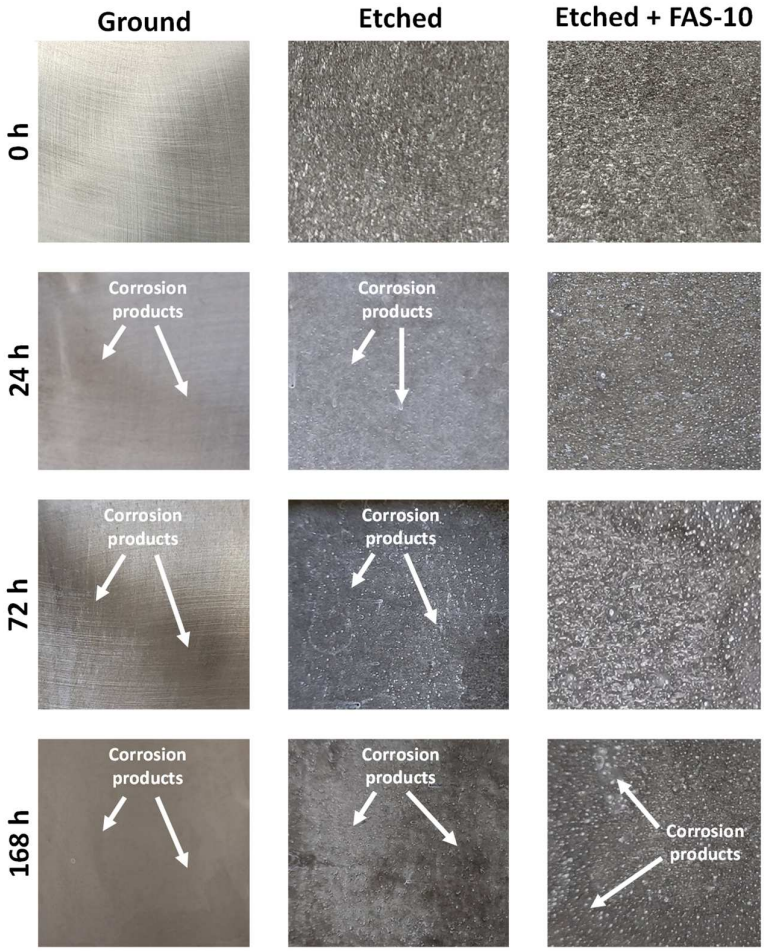

Figure 8. The surface appearance of ground and treated aluminium surfaces (etched for 30 s in 0.5 M $CuCl_2$ etched and grafted for 30 min in 1 wt.% ethanol FAS-10 solution) after selected times during the corrosion test in a salt spray chamber, ASTM B117. The white arrows mark the positions where corrosion products were noticed.

Poor corrosion resistance was also observed on the etched sample (Figure 8). After 24 h of exposure, numerous corrosion products (white spots) were already evident. The quantity of these products was much higher than on the ground surface, confirming the

slightly inferior corrosion resistance of etched aluminium. This can be the result of several factors: (i) enhanced surface roughness and surface great wettability (ii) less efficient surface passivation, and (iii) presence of residual copper and copper deposits after etching. The amount of corrosion products increased with exposure time, particularly after 72 and 168 h (Figure 8).

Improved corrosion resistance was detected on FAS-modified aluminium. The superhydrophobic surface prevented contact between the corrosive medium and the aluminium surface, hindering the reaction between the NaCl solution and the aluminium. However, even in this case, the surface was not completely protected, as individual corrosion sites were detected after 168 h (Figure 8). Nonetheless, the number of corrosion sites was much smaller than that of the ground or etched surfaces, confirming the improved protection against corrosion of aluminium. This observation is consistent with the electrochemical data presented in Figure 7.

The test confirmed that surface modification significantly improves corrosion protection compared to ground aluminium. However, the stability of such a surface is still inadequate to meet the standards that require complete protection for over 500 h. Despite this drawback, the results are very promising, considering the thin nature of the FAS-10 layer. Preventing the contact of the corrosive medium with the surface remains an effective method of corrosion protection.

3.6. Enhancement of Anti-Icing Behaviour

The results of ice nucleation temperature are shown in Figure 9 in the form of probability density histograms for both evaluated surfaces. Data is binned into 0.5 K wide bins centred around temperatures between −14.5 °C and −22.5 °C. Additionally, a Kernel fit as calculated in MathWorks MATLAB R2021b is shown for both distributions. The superhydrophobic etched surface (FAS-10) provided a lower average nucleation temperature of −19.8 °C ± 1.8 K compared to the untreated aluminium surface (−18.1 °C ± 1.6 K). In both cases, the distribution is not symmetrical since some droplets freeze earlier (i.e., at higher temperatures), thus extending the left tail of the distribution. The right tail is significantly shorter as few droplets freeze at significantly lower temperatures compared to the average nucleation temperature. Overall, the functionalised surface provides roughly 2 K lower average nucleation temperature in comparison with the untreated surface, meaning it can function in colder environments with reduced risk of nucleation of water droplets that may be present on a subcooled surface.

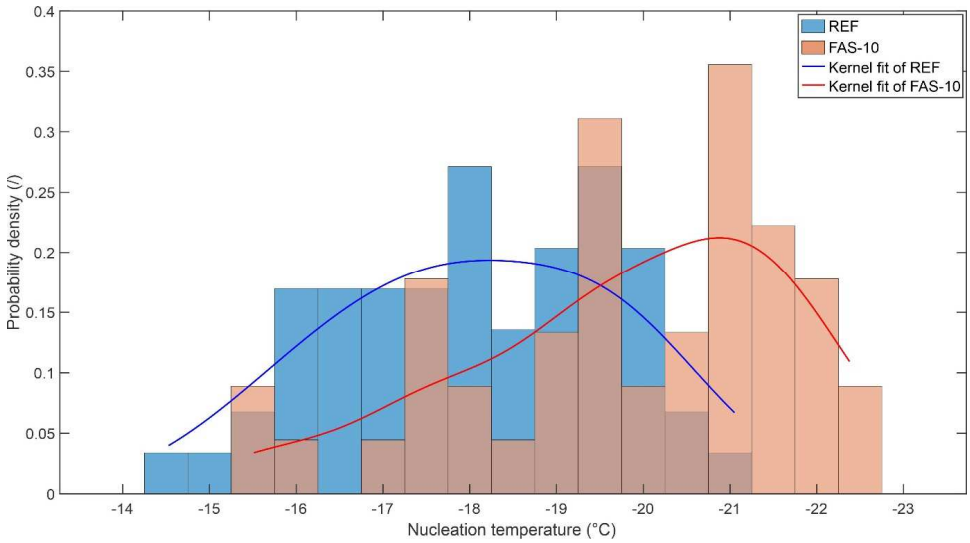

Figure 9. Probability density histograms and Kernel fits of the ice nucleation temperature on the untreated reference surface (REF) and on the superhydrophobic etched FAS-10 surface. Brown colour represents overlapping between blue and ocher colours.

Evaluation of the freezing delay revealed that the superhydrophobic etched surface provides a notably longer delay time in comparison with the untreated surface, as is evident from the results in Figure 10. This can be mainly attributed to the smaller contact area between the solid surface and the liquid droplet undergoing cooling since the solid-liquid contact area is significantly reduced in the Cassie-Baxter heterogeneous wetting regime, which is present on the FAS-10 surface. Furthermore, due to the droplet's shape, the projected contact area is also smaller for the FAS-10 surface compared to the untreated reference surface. These two effects contribute to the freezing delay being over 500% longer on the FAS-10 surface at −15 °C and over 200% longer at −17.5 °C. At −20 °C, which is below the average nucleation temperature for the REF surface and roughly matches the average nucleation temperature of the FAS-10 surface, the difference in freezing delay is smaller since many droplets freeze before the target temperature is reached.

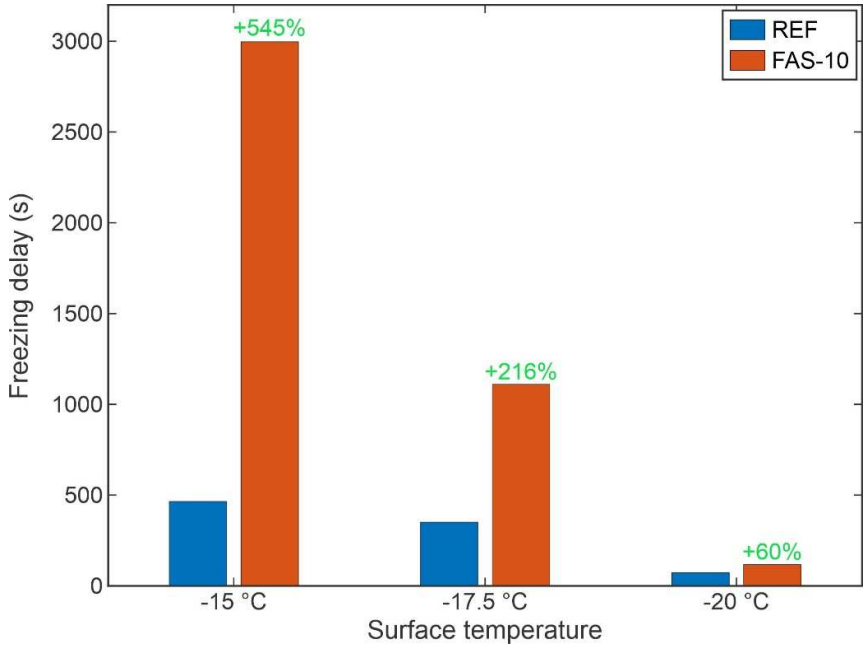

Figure 10. Freezing delay on the untreated reference surface (REF) and on the superhydrophobic etched FAS-10 surface at three surface temperatures. The relative enhancement is provided in green text.

Due to the limited interaction between water droplets and the metal substrate, superhydrophobic surfaces notably influence (de)icing dynamics. This investigation involved comparative analyses on ground and optimised (etched and grafted with FAS-10) superhydrophobic aluminium samples (Figure 11).

The findings underscore a substantial prolongation of de-icing durations on superhydrophobic surfaces compared to the ground sample. Specifically, while droplets on the ground surface melt within 90 s, those on the superhydrophobic surface remain frozen. This discrepancy primarily stems from the heat exchange mechanisms between the surface and the water droplet. In instances of heightened wettability, substantial surface contact of the droplet facilitates convective heat transfer.

This observed melting delay aligns with thermodynamic principles. The droplet on the cold surface mainly acquires heat from the surrounding air through convection and thermal radiation, while it also absorbs heat via conduction from contact with the solid surface [31,56]. Thus, it can explain why a droplet suspended on the superhydrophobic surface (treated aluminium) takes longer to melt than on the ground surface.

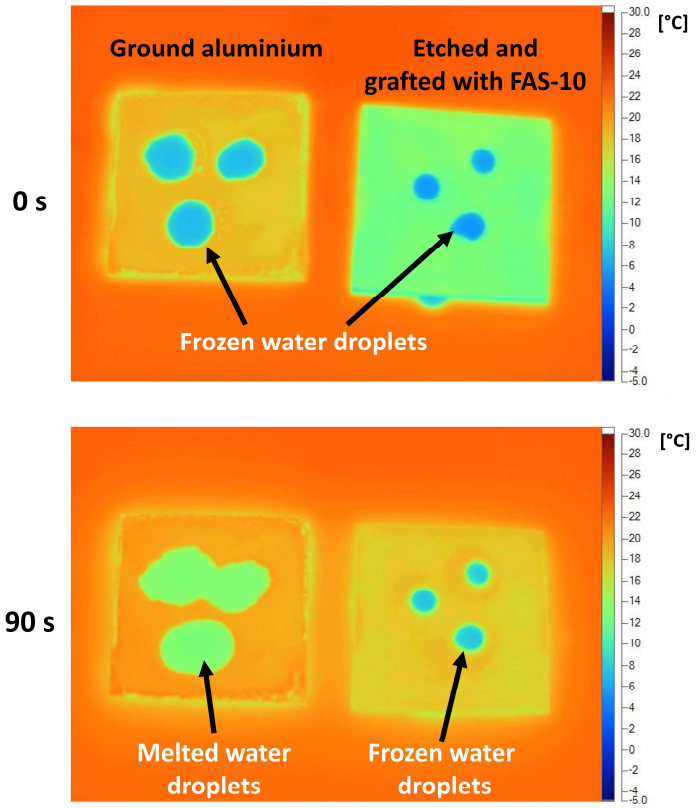

Figure 11. Frames depicting the deicing process on both ground and treated aluminium surfaces after samples were taken from the freezer (−15 °C) and exposed to ambient temperature. The frames were captured using an infrared thermal camera at selected intervals (0 and 90 s).

These findings confirmed that superhydrophobic aluminium exhibits high anti-icing potential, characterised by delayed icing on the treated aluminium surface.

4. Conclusions

A (super)hydrophobic aluminium surface has been successfully created through a straightforward and cost-effective two-step process involving chemical etching in $CuCl_2$ solution followed by grafting with perfluoroalkyl silane (FAS-10).

The weight loss and surface topography analyses confirm that $CuCl_2$ significantly enhances the etching of aluminium, with the effect being dependent on concentration. The roughening of the aluminium surface via etching in $CuCl_2$ solution emerges as a critical parameter, facilitating the formation of a micro/nano-pattern and aluminium oxide/hydroxide structure, which serves as an active surface for subsequent grafting with the perfluoroalkyl silane film.

Optimal results were achieved with an etching time of 30 s followed by 30 min of grafting in FAS-10 solution, resulting in a superhydrophobic aluminium surface with a water contact angle exceeding 150° and a low sliding angle of less than 10°. Electrochemical and salt spray tests confirmed that the superhydrophobic surface enhances corrosion protection due to the formation of a barrier that prevents contact between the aluminium surface and the corrosion medium.

The superhydrophobic aluminium surface exhibits remarkable dynamic properties, characterised by a bouncing effect that leaves no residual water on the surface, indicating excellent self-cleaning capabilities. An average ice nucleation temperature of −19.8 °C was also measured on the superhydrophobic surface, marking a ~2 K reduction compared to the untreated surface. The freezing delay was also significantly increased on the superhydrophobic surface, with a recorded increase of 545% and 216% at −15 °C and −17.5 °C,

respectively. The reduced contact of water droplets with the treated surface leads to slower heat transfer between the droplet and the surface, delaying cooling, ice nucleation, and droplet melting, confirming an improved anti-icing performance.

Given these properties, the fabricated aluminium surface is a promising candidate for various applications, enhancing the durability and functionality of aluminium when exposed to real-world environments.

Author Contributions: Conceptualisation, P.R. and M.M.; methodology, P.R. and M.M.; validation, P.R., M.M., I.G. and I.M.; formal analysis, P.R. and M.M.; data curation, P.R. and M.M.; writing—original draft preparation, P.R. and M.M.; writing—review and editing, P.R., M.M., I.G. and I.M.; supervision, I.G. and I.M.; funding acquisition, P.R., M.M., I.G. and I.M. All authors have read and agreed to the published version of the manuscript.

Funding: The financial support from the Slovenian Research and Innovation Agency is acknowledged: research core funding No. P2-0393, P1-0134, and P2-0223.

Data Availability Statement: The raw data supporting the conclusions of this article will be made available by the authors on request.

Acknowledgments: The authors acknowledge Primož Fajdiga, for his valuable technical assistance in performing the anti-icing test with the thermal camera and Barbara Kapun for performing SEM/EDS analysis. The authors also acknowledge Mija Kapun and Daniil Gainullov for technical assistance during sample preparation and Grega Celcar from the Gymnasium Jože Plečnik, Ljubljana.

Conflicts of Interest: The authors declare no conflicts of interest.

References

1. Hatch, J.E. *Aluminum: Properties and Physical Metallurgy*; ASM International: Almere, The Netherlands, 1984; ISBN 1-61503-169-3.
2. Brough, D.; Jouhara, H. The Aluminium Industry: A Review on State-of-the-Art Technologies, Environmental Impacts and Possibilities for Waste Heat Recovery. *Int. J. Thermofluids* 2020, *in press*. [CrossRef]
3. Czerwinski, F. Current Trends in Automotive Lightweighting Strategies and Materials. *Materials* **2021**, *14*, 6631. [CrossRef] [PubMed]
4. The Surface Treatment and Finishing of Aluminum and Its Alloys, 6th Edition. Available online: https://www.asminternational.org/books-and-handbooks/results/-/journal_content/56/10192/06945G/PUBLICATION/ (accessed on 8 December 2023).
5. Martin, F.J.; Cheek, G.T.; O'Grady, W.E.; Natishan, P.M. Impedance Studies of the Passive Film on Aluminium. *Corros. Sci.* **2005**, *47*, 3187–3201. [CrossRef]
6. Mansfeld, F.; Chen, C.; Breslin, C.B.; Dull, D. Sealing of Anodized Aluminum Alloys with Rare Earth Metal Salt Solutions. *J. Electrochem. Soc.* **1998**, *145*, 2792–2798. [CrossRef]
7. Bouchama, L.; Azzouz, N.; Boukmouche, N.; Chopart, J.P.; Daltin, A.L.; Bouznit, Y. Enhancing Aluminum Corrosion Resistance by Two-Step Anodizing Process. *Surf. Coat. Technol.* **2013**, *235*, 676–684. [CrossRef]
8. Becker, M. Chromate-Free Chemical Conversion Coatings for Aluminum Alloys. *Corros. Rev.* **2019**, *37*, 321–342. [CrossRef]
9. Kendig, M.; Jeanjaquet, S.; Addison, R.; Waldrop, J. Role of Hexavalent Chromium in the Inhibition of Corrosion of Aluminum Alloys. *Surf. Coat. Technol.* **2001**, *140*, 58–66. [CrossRef]
10. Gharbi, O.; Ogle, K.; Han, J. On the Chemistry of Conversion Coatings. In *Encyclopedia of Solid-Liquid Interfaces*, 1st ed.; Wandelt, K., Bussetti, G., Eds.; Elsevier: Oxford, UK, 2024; pp. 532–546. ISBN 978-0-323-85670-6.
11. dos Santos, F.C.; Pulcinelli, S.H.; Santilli, C.V.; Hammer, P. Protective PMMA-Silica Coatings for Aluminum Alloys: Nanostructural Control of Elevated Thermal Stability and Anticorrosive Performance. *Prog. Org. Coat.* **2021**, *152*, 106129. [CrossRef]
12. Rodič, P.; Lekka, M.; Andreatta, F.; Fedrizzi, L.; Milošev, I. The Effect of Copolymerisation on the Performance of Acrylate-Based Hybrid Sol-Gel Coating for Corrosion Protection of AA2024-T3. *Prog. Org. Coat.* **2020**, *147*, 105701. [CrossRef]
13. Rodič, P.; Korošec, R.C.; Kapun, B.; Mertelj, A.; Milošev, I. Acrylate-Based Hybrid Sol-Gel Coating for Corrosion Protection of AA7075-T6 in Aircraft Applications: The Effect of Copolymerization Time. *Polymers* **2020**, *12*, 948. [CrossRef]
14. Li, W.; Zhan, Y.; Yu, S. Applications of Superhydrophobic Coatings in Anti-Icing: Theory, Mechanisms, Impact Factors, Challenges and Perspectives. *Prog. Org. Coat.* **2021**, *152*, 106117. [CrossRef]
15. Huang, W.; Huang, J.; Guo, Z.; Liu, W. Icephobic/Anti-Icing Properties of Superhydrophobic Surfaces. *Adv. Colloid Interface Sci.* **2022**, *304*, 102658. [CrossRef] [PubMed]
16. He, Q.; Xu, Y.; Zhang, F.; Jia, Y.; Du, Z.; Li, G.; Shi, B.; Li, P.; Ning, M.; Li, A. Preparation Methods and Research Progress of Super-Hydrophobic Anti-Icing Surface. *Adv. Colloid Interface Sci.* **2024**, *323*, 103069. [CrossRef] [PubMed]
17. Zhang, D.; Wang, L.; Qian, H.; Li, X. Superhydrophobic Surfaces for Corrosion Protection: A Review of Recent Progresses and Future Directions. *J. Coat. Technol. Res.* **2016**, *13*, 11–29. [CrossRef]

18. Barati Darband, G.; Aliofkhazraei, M.; Khorsand, S.; Sokhanvar, S.; Kaboli, A. Science and Engineering of Superhydrophobic Surfaces: Review of Corrosion Resistance, Chemical and Mechanical Stability. *Arab. J. Chem.* **2018**, *13*, 1763–1802. [CrossRef]
19. Zhan, Z.; Li, Z.; Yu, Z.; Singh, S.; Guo, C. Superhydrophobic Al Surfaces with Properties of Anticorrosion and Reparability. *ACS Omega* **2018**, *3*, 17425–17429. [CrossRef]
20. Farag, A.A.; Mohamed, E.A.; Toghan, A. The New Trends in Corrosion Control Using Superhydrophobic Surfaces: A Review. *Corros. Rev.* **2023**, *41*, 21–37. [CrossRef]
21. Yang, Q.; Cao, J.; Ding, R.; Zhan, K.; Yang, Z.; Zhao, B.; Wang, Z.; Ji, V. The Synthesis and Mechanism of Superhydrophobic Coatings with Multifunctional Properties on Aluminum Alloys Surface: A Review. *Prog. Org. Coat.* **2023**, *184*, 107875. [CrossRef]
22. Bahgat Radwan, A.; Abdullah, A.M.; Alnuaimi, N.A. Recent Advances in Corrosion Resistant Superhydrophobic Coatings. *Corros. Rev.* **2018**, *36*, 127–153. [CrossRef]
23. Tong, W.; Xiong, D.; Wang, N.; Yan, C.; Tian, T. Green and Timesaving Fabrication of a Superhydrophobic Surface and Its Application to Anti-Icing, Self-Cleaning and Oil-Water Separation. *Surf. Coat. Technol.* **2018**, *352*, 609–618. [CrossRef]
24. Vazirinasab, E.; Jafari, R.; Momen, G. Application of Superhydrophobic Coatings as a Corrosion Barrier: A Review. *Surf. Coat. Technol.* **2018**, *341*, 40–56. [CrossRef]
25. Shirtcliffe, N.J.; McHale, G.; Atherton, S.; Newton, M.I. An Introduction to Superhydrophobicity. *Adv. Colloid Interface Sci.* **2010**, *161*, 124–138. [CrossRef]
26. Rodič, P.; Kapun, B.; Milošev, I. Superhydrophobic Aluminium Surface to Enhance Corrosion Resistance and Obtain Self-Cleaning and Anti-Icing Ability. *Molecules* **2022**, *27*, 1099. [CrossRef]
27. Rodič, P.; Milošev, I. One-Step Ultrasound Fabrication of Corrosion Resistant, Self-Cleaning and Anti-Icing Coatings on Aluminium. *Surf. Coat. Technol.* **2019**, *369*, 175–185. [CrossRef]
28. Kumar, A.; Gogoi, B. Development of Durable Self-Cleaning Superhydrophobic Coatings for Aluminium Surfaces via Chemical Etching Method. *Tribol. Int.* **2018**, *122*, 114–118. [CrossRef]
29. Mohamed, A.M.A.; Abdullah, A.M.; Younan, N.A. Corrosion Behavior of Superhydrophobic Surfaces: A Review. *Arab. J. Chem.* **2015**, *8*, 749–765. [CrossRef]
30. Cao, L.; Jones, A.K.; Sikka, V.K.; Wu, J.; Gao, D. Anti-Icing Superhydrophobic Coatings. *Langmuir* **2009**, *25*, 12444–12448. [CrossRef] [PubMed]
31. Rodič, P.; Kapun, B.; Panjan, M.; Milošev, I. Easy and Fast Fabrication of Self-Cleaning and Anti-Icing Perfluoroalkyl Silane Film on Aluminium. *Coatings* **2020**, *10*, 234. [CrossRef]
32. Milošev, I.; Bakarič, T.; Zanna, S.; Seyeux, A.; Rodič, P.; Poberžnik, M.; Chiter, F.; Cornette, P.; Costa, D.; Kokalj, A.; et al. Electrochemical, Surface-Analytical, and Computational DFT Study of Alkaline Etched Aluminum Modified by Carboxylic Acids for Corrosion Protection and Hydrophobicity. *J. Electrochem. Soc.* **2019**, *166*, C3131–C3146. [CrossRef]
33. Lakshmi, R.V.; Bharathidasan, T.; Basu, B.J. Superhydrophobic Sol-Gel Nanocomposite Coatings with Enhanced Hardness. *Appl. Surf. Sci.* **2011**, *257*, 10421–10426. [CrossRef]
34. Saji, V.S. Superhydrophobic Surfaces and Coatings by Electrochemical Anodic Oxidation and Plasma Electrolytic Oxidation. *Adv. Colloid Interface Sci.* **2020**, *283*, 102245. [CrossRef]
35. Song, J.; Xu, W.; Liu, X.; Wei, Z.; Lu, Y. Fabrication of Superhydrophobic Cu Surfaces on Al Substrates via a Facile Chemical Deposition Process. *Mater. Lett.* **2012**, *87*, 43–46. [CrossRef]
36. Çakır, O. Chemical Etching of Aluminium. *J. Mater. Process. Technol.* **2008**, *199*, 337–340. [CrossRef]
37. Zhang, Y.; Wu, J.; Yu, X.; Wu, H. Low-Cost One-Step Fabrication of Superhydrophobic Surface on Al Alloy. *Appl. Surf. Sci.* **2011**, *257*, 7928–7931. [CrossRef]
38. Liao, R.; Zuo, Z.; Guo, C.; Yuan, Y.; Zhuang, A. Fabrication of Superhydrophobic Surface on Aluminum by Continuous Chemical Etching and Its Anti-Icing Property. *Appl. Surf. Sci.* **2014**, *317*, 701–709. [CrossRef]
39. Newman, L. Etching of Aluminum and Its Alloys. In *Aluminum Science and Technology*; ASM International: Almere, The Netherlands, 2018. [CrossRef]
40. Song, J.; Xu, W.; Liu, X.; Lu, Y.; Wei, Z.; Wu, L. Ultrafast Fabrication of Rough Structures Required by Superhydrophobic Surfaces on Al Substrates Using an Immersion Method. *Chem. Eng. J.* **2012**, *211*, 143–152. [CrossRef]
41. Fenero, M.; Knez, M.; Saric, I.; Petravic, M.; Grande, H.; Palenzuela, J. Omniphobic Etched Aluminum Surfaces with Anti-Icing Ability. *Langmuir* **2020**, *36*, 10916–10922. [CrossRef]
42. Han, S.W.; Jeong, J.; Lee, D.H. Ice-Phobic Behavior of Superhydrophobic Al Surface Undervarious Etching Conditions. *J. Electroceramics* **2014**, *33*, 82–88. [CrossRef]
43. Peng, H.; Luo, Z.; Li, L.; Xia, Z.; Du, J.; Zheng, B. Facile Fabrication of Superhydrophobic Aluminum Surfaces by Chemical Etching and Its Anti-Icing/Self-Cleaning Performances. *Mater. Res. Express* **2019**, *6*, 096586. [CrossRef]
44. Ruan, M.; Li, W.; Wang, B.; Deng, B.; Ma, F.; Yu, Z. Preparation and Anti-Icing Behavior of Superhydrophobic Surfaces on Aluminum Alloy Substrates. *Langmuir* **2013**, *29*, 8482–8491. [CrossRef]
45. Wang, Y.; Xue, J.; Wang, Q.; Chen, Q.; Ding, J. Verification of Icephobic/Anti-Icing Properties of a Superhydrophobic Surface. *ACS Appl. Mater. Interfaces* **2013**, *5*, 3370–3381. [CrossRef] [PubMed]
46. Saleema, N.; Sarkar, D.K.; Gallant, D.; Paynter, R.W.; Chen, X.-G. Chemical Nature of Superhydrophobic Aluminum Alloy Surfaces Produced via a One-Step Process Using Fluoroalkyl-Silane in a Base Medium. *ACS Appl. Mater. Interfaces* **2011**, *3*, 4775–4781. [CrossRef] [PubMed]

47. *ISO 25178-1:2016*; Geometric Product Specifications (GPS)—Surface Texture: Areal, Edition 1, 2016. International Organization for Standardization: Geneva, Switzerland, 2016.
48. Baboian, R. *Corrosion Tests and Standards: Application and Interpretation*; ASTM International: Almere, The Netherlands, 2005.
49. *ASTM D117-22*; Standard Practice for Operating Salt Spray (Fog) Apparatus. ASTM International: West Conshohocken, PA, USA, 2022.
50. Pourbaix, M. *Atlas of Electrochemical Equilibria in Aqueous Solutions*; National Association of Corrosion Engineers: Houston, TX, USA, 1974.
51. Patil, D.H.; Thorat, S.B.; Khake, R.A.; Mudigonda, S. Comparative Study of $FeCl_3$ and $CuCl_2$ on Geometrical Features Using Photochemical Machining of Monel 400. *Procedia CIRP* **2018**, *68*, 144–149. [CrossRef]
52. Rao, P.N.; Kunzru, D. Fabrication of Microchannels on Stainless Steel by Wet Chemical Etching. *J. Micromechanics Microengineering* **2007**, *17*, N99–N106. [CrossRef]
53. Poberžnik, M. Quantum Mechanical Modeling of the Oxidation of Aluminum Surfaces and Their Interactions with Corrosion Inhibitors. Ph.D. Thesis, University of Ljubljana, Ljubljana, Slovenia, 2019. Volume 2019. pp. 75–83.
54. Poberžnik, M.; Costa, D.; Hemeryck, A.; Kokalj, A. Insight into the Bonding of Silanols to Oxidized Aluminum Surfaces. *J. Phys. Chem. C* **2018**, *122*, 9417–9431. [CrossRef]
55. Rodič, P.; Milošev, I. Corrosion Inhibition of Pure Aluminium and Alloys AA2024-T3 and AA7075-T6 by Cerium(III) and Cerium(IV) Salts. *J. Electrochem. Soc.* **2016**, *163*, C85–C93. [CrossRef]
56. Shen, Y.; Tao, J.; Tao, H.; Chen, S.; Pan, L.; Wang, T. Superhydrophobic Ti6Al4V Surfaces with Regular Array Patterns for Anti-Icing Applications. *RSC Adv.* **2015**, *5*, 32813–32818. [CrossRef]